# Sintering Behavior of BST Nanoparticles at Low Temperature and Electrical Properties of their Ceramics

**Jianquan Qi** ( jianquanqi@mail.tsinghua.edu.cn )
Northeast Unv at Qinhuangdao

**Yan Li**
Neuq

**Mengyin Li**
Neuq

**Jiahui Xie**
NEUQ

**Tianchi Yu**
NEUQ

**Qingwen Sun**
NEUQ

**Yifan Yan**
neuq

**Jian Wang**
NEUQ

**Xinkai Xiong**
NEUQ

**Tinghui Wang**
NEUQ

**Xiumei Han**
NEUQ

**Research Article**

**Keywords:** BST, Sintering, Electrical property, Nanoparticles, Direct synthesis

**Posted Date:** July 8th, 2020

**DOI:** https://doi.org/10.21203/rs.3.rs-40548/v1

# Abstract

The powders of the $Ba_{0.75}Sr_{0.25}TiO_3$ (BST) nanoparticles were directly synthesized by milling of $Ba(OH)_2{\cdot}8H_2O$, $Sr(OH)_2{\cdot}8H_2O$ and $Ti(BuO)_4$ in ethanol at room temperature. They have homogenous grains of ~15 nm and the high sintering activity. The dense ceramics with the density >90% can be obtained at a sintering temperature of ≤950 $^oC$ by them with adding 3 wt% sintering aids of $Bi_2O_3$ and $Li_2CO_3$. The sintering behavior of the BST nanoparticles by adding the aids of $Bi_2O_3$ and $Li_2CO_3$ is studied carefully. Several Bi-related compounds are involved in the sintering procedure at a different temperature. They enhance the mass transfer and promote the sintering densification. These compounds such as $Ba_2BiO_4$ and $SrBiO_4$ appear at 800 $^oC$, $LiBa_4Bi_3O_{11}$ and $Sr_{1.2}Bi_{0.8}O_3$ appear over 830 $^oC$, and $Bi_{8.11}Ba_{0.89}O_{13.05}$ appears at 950 $^oC$. The cation Bi in the ceramics has mixture valences of 3+ and 5+. It makes the ceramics as semiconducting state with the dark gray color and decreases the ceramics resistivities. With the sintering temperature increase, especially at 950 $^oC$, the cation Bi tends back to single valence of +3 in the ceramics. The most of alkaline earth cations in Bi-related compounds will release and resorb into the lattice of BST and drive the densification of the nanoparticles. The BST ceramics can have a peak dielectric constant >6500 at 53 $^oC$, loss <0.025, and resistivity >$10^{12}$ W·cm when sintered at a temperature of ≥900 $^oC$ with 3 wt% sintering aids. They have a potential application for multiple layer ceramic capacitors (MLCC) with silver inner-electrodes.


# Introduction

With the development of electrical and electronic industry, higher performance of electrical devices with smaller size and lower cost are demanded. At the same time, more and more attention is paid to environmental protection during fabrication of these devices, such as no pollutant discharge, low energy consumption to control carbon emission, etc.

$Ba_{1-x}Sr_xTiO_3$ (BST) ceramics have high performance in electrical devices. As a solid solution of two typical perovskite ferroelectrics $BaTiO_3$ and $SrTiO_3$, BST can modulate its Curie temperature continuously by the compositions, and thus control its properties desirably [1]. With high dielectric permittivity, low loss, outstanding ferroelectricity, it has attracted attention for decades on the application of a high-voltage capacitor [2], tunable filter, detector [3–4], piezoelectrics [5], sensor [6], pressure transducer and actuator [7], optoelectronic device [8], etc. Especially, the high capacity capacitors based on BST ceramics are indispensable devices in the electronic and electrical circuit for energy storage with high power density [9]. Also the positive temperature resistance (PTCR) [10] based on semiconducting BST ceramics have applied widely for temperature sensors and current control devices. However, the high temperature over 1300 $^oC$ is often necessary to sinter the dense BST ceramics, and thus leads to abnormal graingrowth and properties deterioration [11]. To keep a high temperature for sintering, the energy consumed by the kiln is high because it is proportional to $T^4$ as Stefan-Boltzmann law which determines the blackbody

radiation [12]. To obtain high performance of the ceramics and save much energy, it is necessary to lower the sintering temperature of the BST ceramics.

For the multiple layer ceramic devices (MLCD), the inner metal electrodes must be co-fired with the ceramics so we should adopt Pd or Pt as inner electrodes that can bear the sintering temperature above 1300 $^{o}$C. If the dense ceramics can be sintered at the low temperature < 960 $^{o}$C (silver melting point), the relatively cheap electrodes Ag can be suitable and the total price of the electrical devices can be decreased distinctly.

To control the microstructures and the properties, the ceramics should be sintered at the low temperature. At this time, the graingrowth during sintering can be efficiently controlled and the fine-grain sized ceramics would be obtained. We can decrease the depth of the single layer of MLCD, increase the number of the layers, and thus improve the properties especially as breakdown voltages of the ceramics.

There are several documents on the low temperature sintering of BST ceramics. Unfortunately, they documented the deteriorated properties of the ceramics or did not report them [13, 14]. In this study, we directly synthesized high active BST nanoparticles at room temperature. Adopt $Bi_2O_3$ and $Li_2CO_3$ as sintering aids to sinter the BST ceramics at the low temperature < 960 $^{o}$C for a potential application on silver inner-electrode multiple layer ceramic capacitors (MLCC). The sintering mechanism is also analyzed carefully.

# Experimental Procedure

To sinter the ceramics at low temperatures, the powders of BST nanoparticles should have fine grains to ensure their high activity. We directly synthesized them at room temperature, just similar to synthesize $BaTiO_3$ nanopaticles [15]. In this study, we give a typical example of BST as $Ba_{0.75}Sr_{0.25}TiO_3$ (also abbreviated as BST).

We adopted Barium octahydrate ($Ba(OH)_2{\cdot}8H_2O$), strontium octahydrate ($Sr(OH)_2{\cdot}8H_2O$), and tetrabutyl titanate ($Ti(OC_4H_9)_4$) as starting reagents to prepare the BST nanoparticles. We obtained the titanium solution by dissolving 34.0 g $Ti(OC_4H_9)_4$ into 50 ml absolute ethanol, the base slurry by ball milling 23.7 g $Ba(OH)_2{\cdot}8H_2O$ and 6.65 g $Sr(OH)_2{\cdot}8H_2O$ in 100 ml ethanol for 4 h. We added the titanium solution into the base slurry in the jar and then resealed for another 18 h milling at the rate of 200 rpm. After that, we obtained the white slurry and then the BST nanoparticles by followed air-dry. To study the role of the sintering aids, we added the mixture of $Li_2CO_3$ and $Bi_2O_3$ to the as-prepared BST powders with different contents from 2 to 5 wt%, dry pressed them into disks, and then sintered at different temperatures from 800 to 950 $^{o}$C.

All the samples were analyzed through X-ray diffraction (XRD, X'Pert-Pro MPD, Panalytical Ltd., Holland) using CuKα radiation (40 kV, 30 mA) and field emission scanning electron microscopy (FE-SEM, supra55, Zeiss, Germany). After both surfaces of the ceramic samples were coated with silver paste and sintered

at 800 $^{o}$C for 10 min, the dielectricities of them were measured by Precision LCR Meter (Keysight Technologies, America, E4980A), and the I-V characteristics by High Resistance Meter (Keithley, America, 2400).

# Results And Discussion

It is well known that the higher sintering temperature of the ceramics brings in the more energy consumption. To keep a certain sintering temperature, the energy consumed by the kiln is proportional to $T^4$ as Stefan-Boltzmann law which determines the blackbody radiation. To decrease the sintering temperature and save energy, we need fine grain size nanoparticles of the BST ceramic powders to ensure their high activity. We directly synthesized them at room temperature. The XRD pattern of them is shown in Fig. 1. It is confirmed that the as-prepared nanoparticles have perfect perovskite structures as indexed according to PDF#31–0174. The very weak peak of the impurity phase at 24 $^{o}$ is indexed as $BaCO_3$. The slight amount of $BaCO_3$ in the as-prepared samples possibly derives from the raw material barium hydroxides, which can react with $CO_2$ in the air during its storage. The peaks shift left as a comparison of the theoretical positions, and thus the lattice cell expanded because of hydrogen interstitial and nanoscale size effect. The nanoscale size effect also broadens the peaks of the nanoparticles as we discussed previously [15].

The SEM image of the as-prepared powders is shown in Fig. 2. The average grain size can be estimated at ~ 15 nm. It is following the calculated result by Scherrer's Equation from the XRD peak broadening effect. The nanoparticles agglomerated severely for their high activity. Some sintering aids are necessary to sinter the ceramics at low temperatures because we can hardly eliminate the pores in the inner of the agglomerations.

The ceramic samples sintered at 800 $^{o}$C with different contents of sintering aids are shown in Fig. 3. The sample with 2 wt% sintering aids has a white color. Others have a gray color and get darker and darker with the content of sintering aids. The sintering shrinkages and relative densities of the samples are shown in Fig. 4. It reaches the maximum of both shrinkages and the density with 4 wt% sintering aids. This means that the sintering process at 800 $^{o}$C can be promoted with the sintering aids lower than 4 wt%, and above that, it can be repressed mildly.

The SEM of the samples sintered at 800 $^{o}$C for 8 h with different contents of sintering aids are shown in Fig. 5. It is shown that the grain size of the ceramics decreases with the contents of the sintering aids. Meanwhile, the size of the pores in ceramics also decreases. It means that during the sintering process, the mass transfer and the followed expansion of the grain boundary are repressed by the increase of the aids content, and thus the graingrowth is depressed to obtain the fine grain size ceramics. Opposite to above, the density of the ceramics increases with the content of sintering aids at the beginning. Therefore, it is a benefit for the elimination of the pores and the densification of the ceramics if the sintering aids increase. The mass transfer promotes the densification in the traditional sintering

mechanism, but the repressed mass transfer yields the promoted densification in this system when the sintering aids increase. It is a contradiction with the traditional sintering mechanism. There must be some new one except for traditional graingrowth, such as, suppose a certain force to close the distance between two nanoparticles to drive the sintering. In Fig. 4, the density and the sintering shrinkage of the samples increases with the content at first, reaches a maximum at 4 wt%, and then decreases slightly after that. To clarify the supposition, the XRD patterns of the ceramic samples added with 3 and 5 wt% sintering aids are shown in Fig. 6. There are two impurity phases indexed in the patterns, main impurity phase: $SrBiO_3$ (PDF#48–0321) and other: $Ba_2BiO_4$ (PDF#46–0088). They both are distorted perovskite structures and display superconductivity [16]. $SrBiO_3$ can be expressed as $SrBi_{0.5}^{3+}Bi_{0.5}^{5+}O_3$ [17], and $Ba_2BiO_4$ is described as the probable end member ($x = 0.67$) of an oxygen-defect series the generic formula of $Ba_2(Bi_{1-x}^{3+}Ba_x)Bi^{5+}O_{6-\delta}$ as double perovskite structure [18]. The peak of $SrBiO_3$ is much stronger than that of $Ba_2BiO_4$ as shown as the inset of Fig. 6. It is realized that $Ba_2BiO_4$ is more difficult to form than $SrBiO_3$, although Ba content is much higher than Sr in our BST ($Ba_{0.75}Sr_{0.25}TiO_3$) nanoparticles. The relative content of $Ba_2BiO_4$ vs $SrBiO_3$ increases with the content of the sintering aids. The mismatched ratio of $Ba_2BiO_4$ vs BST is higher than that of $SrBiO_3$ vs BST because Bi and Ba have a bigger ion radius than Ti, $Ba_2BiO_4$ has bigger perovskite cell than $SrBiO_3$ and they both have bigger cell than BST. For all of them are perovskite structure, the Bi-related perovskites grow epitaxially on the surface of BST nanoparticles, and close them together to make the sintering densification without mass transfer from one BST nanoparticle to another.

To study the influence of the temperature on the sintering procedure, the sample added with 3 wt% sintering aids is sintered at different temperatures from 800 to 950 $^oC$. The ceramic samples are shown in Fig. 7. They have a gray color with a sintering temperature of 800 ~ 900 $^oC$. The color of them gets darker and darker till 850 $^oC$, becomes shallow at 900 $^oC$, and then changes to yellow at 950 $^oC$. The sintering shrinkages and relative densities of the samples are shown in Fig. 8. They both increase with the sintering temperature approximately. The density can reach > 90% above 900 $^oC$.

The SEM of the samples sintered at different temperatures is shown in Fig. 9. It is shown that the grain size of the ceramics increases with the temperature. Because the sintering can be promoted with the temperature, the mass transfer is a run-up to make graingrowth.

We should consider another important factor as some efficient sintering impurities involved at a higher temperature than 800 $^oC$. To clarify them, the XRD patterns of the ceramic samples sintered at different temperatures were analyzed carefully. They are shown in Fig. 10. All patterns showed the perfect perovskite structure of BST. To research the impurity phases in them, the patterns were zoomed-in along the Y axle as shown in Fig. 11. As analyzed as previously, in the sample sintered at 800 $^oC$, Bi-related perovskite impurity phases as $SrBiO_3$ and $Ba_2BiO_3$ were indexed. In the sample sintered at 830 $^oC$, new impurity phases of $Sr_{1.262}Bi_{0.737}O_3$ (pdf#48–0508) and $LiBa_4Bi_3O_{11}$ (pdf#46–0634) were indexed. The valence of Bi in $Sr_{1.262}Bi_{0.737}O_3$ is different from that in $SrBiO_3$. Only $Bi^{5+}$ exists in $Sr_{1.262}Bi_{0.737}O_3$ but

both $Bi^{3+}$ and $Bi^{5+}$coexists in $SrBiO_3$. $Sr_{1.262}Bi_{0.737}O_3$ can be expressed as perovskite style as $SrSr_{0.262}Bi_{0.737}{}^{5+}O_3$. $Sr^{2+}$ also can jam into the B-site of $ABO_3$-typed perovskite as discussed previously as partial $Ba^{2+}$ in $Ba_2BiO_4$. In this sample, although $Ba_2BiO_4$ is still indexed, $SrBiO_3$ disappears to turn to $Sr_{1.262}Bi_{0.737}O_3$. The grain size of the sample sintered at 830 $^oC$ increased, but the relative density of it decreased as a comparison of the sample sintered at 800 $^oC$. It may be caused by a single valence of Bi in $Sr_{1.262}Bi_{0.737}O_3$ that it does not good effect on the densification of the ceramic sintering. Furthermore, $Sr_{1.262}Bi_{0.737}O_3$ was rarely reported in the previous documents. $LiBa_4Bi_3O_{11}$ can be expressed as $Ba_4LiBi^{5+}Bi^{3+}Bi^{5+}O_{12-\delta}$ and thus has a tetrad perovskite structure. It can be sintered at 870 ~ 910 $^oC$ as microwave ceramics with dielectric constant as 38 ~ 44 and $Q_f$ as 35000–54000 GHz [19]. For the sample sintered at 850 $^oC$, $LiBa_4Bi_3O_{11}$ was indexed as the main impurity phase and the intensity of $Sr_{1.262}Bi_{0.737}O_3$ decreased rapidly. In the sample sintered at 900 $^oC$, $LiBa_4Bi_3O_{11}$ was also indexed as the main impurity phase and $Sr_{1.262}Bi_{0.737}O_3$ disappeared. In the sample sintered at 950 $^oC$, $Bi_{8.11}Ba_{0.89}O_{13.05}$ (pdf#45–0289) was indexed and the intensity of $LiBa_4Bi_3O_{11}$decreased rapidly. In the samples sintered at all of our temperatures, a trace of $Ba_2BiO_4$ always existed. $Bi_{8.11}Ba_{0.89}O_{13.05}$ can be considered as Ba-doped $Bi_2O_3$ which has not a perovskite structure. It was reported as a secondary phase in the ceramics of the binary system of $BaTiO_3$ and $Bi_2O_3$ [20]. Therefore, most of Bi-related perovskite impurity phases drove the densification of the ceramic sintering. The alkaline earth cations in them were resorbed by the main lattice of BST, and $Bi_2O_3$ phase were released again.

Table 1
The impurity phases indexed in the ceramics sintered at different temperature

| **Sintering temperature** | **$SrBiO_3$ ($Bi^{3+}$, $Bi^{5+}$)** | **$Ba_2BiO_4$ ($Bi^{3+}$, $Bi^{5+}$)** | **$Sr_{1.262}Bi_{0.737}O_3$ ($Bi^{5+}$)** | **$LiBa_4Bi_3O_{11}$ ($Bi^{3+}$, $Bi^{5+}$)** | **$Bi_{8.11}Ba_{0.89}O_{13.05}$ ($Bi^{3+}$)** |
|---|---|---|---|---|---|
| 800 $^oC$ | **X*** | X | | | |
| 830 $^oC$ | | X | **X** | X | |
| 850 $^oC$ | | X | X | **X** | |
| 900 $^oC$ | | X | | **X** | |
| 950 $^oC$ | | X | | X | **X** |
| * red “X” expresses the main impurity phase | | | | | |

The impurity phases indexed in the ceramics sintered at different temperatures are listed in Table 1. Red “X” clearly showed the main impurity phase indexed in the ceramics sintered at a different temperature. The valent states of Bi were also listed in each impurity phases. Overall, three phases of impurities

involved here, $SrBiO_3$, $Ba_2BiO_4$, and $LiBa_4Bi_3O_{11}$ might be taken effect on the densification of ceramic sintering, in which Bi has complex valences. The impurities as $Sr_{1.262}Bi_{0.737}O_3$ and $Bi_{8.11}Ba_{0.89}O_{13.05}$ might be taken little effect on it, in which Bi has a single valence.

The sintering mechanism of BST nanoparticles driven by Bi-related perovskite is illustrated in Fig. 12. For the high vapor pressure of $Bi_2O_3$ near its melting point (817 $^oC$), it is easily vaporized to fill the interspaces among BST nanoparticles shown as big white circles. The alkaline earth cations ($Ba^{2+}$ or $Sr^{2+}$, as shown as small blue circles) immigrated to $Bi_2O_3$ (as shown as orange circles) and partial of $Bi^{3+}$ is oxidized to $Bi^{5+}$ by oxygen in the air. They make epitaxial growth of a layer of Bi-related perovskite along a fixed direction shown as blue lines in the circles on the surface of BST nanoparticles. At this moment, the surfaces of BST nanoparticles near the epitaxial layer carry the negative charges and produce surface charges gathering because of the immigration out of cations. The opposite sides of it carry positive charges for the polarization of the surface charges. The condition of the epitaxial layer is just opposite to that of BST nanoparticles as shown in Fig. 12 (a). Driven with the electrostatic force, the nanoparticles of BST rotate in the same direction and close together as shown in Fig. 12 (b). Vaporized $Bi_2O_3$ from Bi-related perovskites, the most of alkaline earth cations in them are resorbed by the main lattice of BST to drive the nanoparticles close together much more as shown in Fig. 12 (c). At the end of the time, the BST nanoparticles emerged into a single particle as shown in Fig. 12 (d). The densification of the ceramic sintering is driven without mass transfer from one BST nanoparticle to another, and the dense ceramics can be obtained at a low temperature. The mechanism can be considered as the mergence of small particles driven by the intermediate impurity phase of Bi-related perovskite during the sintering.

The small particles merged into a large grain can be observed in the sample sintered insufficiently. Figure 13 showed SEM of the samples sintered at 950 $^oC$ for 2 h with 5 wt% sintering aids. It is observed that the small particles merge into a large grain in Fig. 13 as the condition illustrated in Fig. 12. The small particles can be faintly observed in a large one at left lower in Fig. 13 and also in other large grains. They can grow to normal grains under the sufficient sintering further. Therefore, the sintering mechanism illustrated in Fig. 12 was confirmed.

The I-V curves of the samples sintered at 800 $^oC$ with different contents of the sintering aids are shown in Fig. 14. For the samples behave impure resistances, the curves are not linear. The average resistivities of the samples were estimated as shown in Fig. 15. The leakage currents or conductivities as reciprocal of the resistivities of the samples are related to the conductive secondary phases, pores, and distribution of them in the ceramics. $SrBiO_3$ with superconductivity can behave conductive secondary phase. In $Ba_2BiO_4$, a full $Bi^{3+}$ -$Bi^{5+}$ separation occurs as a result of the simultaneous presence of large $Ba^{2+}$cation both in dodecahedral and octahedral coordination. Barium in an octahedral site breaks the $Bi^{3+}$-O-$Bi^{5+}$ bonding, stabilizes insulating properties, and decreases the conductivity of $Ba_2BiO_4$. These enlighten us that the content of $SrBiO_3$ in ceramics is a crucial factor to influence on the resistivities of the samples in Fig. 15.

In these samples, both the contents of $SrBiO_3$ and $Ba_2BiO_4$ increase with the content of sintering aids, but the content of $Ba_2BiO_4$ increases much rapidly. If a sample has the maximum content of $SrBiO_3$, and it can have the minimum resistivity, such as the sample with 4 wt% sintering aids.

The I-V curves of the samples sintered at different temperatures with 3 wt% sintering aids are shown in Fig. 16. The average resistivities of the samples were estimated as shown in Fig. 17. As we mentioned previously, the $LiBa_4Bi_3O_{11}$ phase can be fabricated as a microwave capacitor, and thus it may have a high resistivity. $Sr_{1.262}Bi_{0.737}O_3$ and $Bi_{8.11}Ba_{0.89}O_{13.05}$ have a single valence of Bi ion in them, and they may not behave a good conductivity. The resistivity of the sample increases with the sintering temperature except the sample sintered at 850 $^oC$.

Because of the decrease of the content of the conductive phase of $SrBiO_3$ and the percentage of pores in the ceramics with the sintering temperature, the resistivity increases with the sintering temperature. For the sample sintered at 850 $^oC$, it has a strange low resistivity. Checked the SEM of it as shown in Fig. 9, much more secondary phase than other samples were observed. The secondary phases behave as irregular particles differently from normal BST grains. Although we cannot confirm the secondary phase belongs to amorphous or what kind of crystalline, it leads to the low resistivity of the ceramics.

The temperature dependences of the dielectricities of the samples sintered at 900 $^oC$ and 950 $^oC$ are shown in Fig. 18. Both of the measured samples behave the typical temperature dependence of the dielectricity of the BST ceramics. They both have a dielectric peak at 53 $^oC$. Assumption the shift efficient of dielectric peak as 2.5 $^oC$/% at Curie point because of $(T_c(BT)-T_c(ST))/100$, where $T_c(BT)$ = 125 $^oC$ and $T_c(ST)$=-125 $^oC$, the dielectric peak of the $Ba_{0.75}Sr_{0.25}TiO_3$ ceramics should locate at 57.5 $^oC$. It is near the experimental value of 53 $^oC$. The peak of the dielectric constant of the sample sintered at 900 $^oC$ ~ 6800 with a loss of 0.01, and that of the sample sintered at 950 $^oC$~ 6300 with a loss of 0.009, respectively. All of their average resistivity > $10^{12}\Omega$•cm and thus we achieved the goal of the sintering at the low temperature < 960$^oC$ (silver melting point) for a potential on silver inner-electrodes MLCC. The dielectric constant of the sample sintered at 900 $^oC$ is higher than that sintered at 950 $^oC$ for the results of the grain size effect on the dielectricity. For the $BaTiO_3$ based ceramics, the dielectric constant reaches their maximum when their grain size ~ 0.5 μm. As we showed SEM of them in Fig. 9, the sample sintered at 900 $^oC$ is just meeting the condition. For the low resistivity of other samples, the dielectricities of others were not measured successfully.

# Conclusions

We directly synthesized BST nanoparticles with a grain size of ~ 15 nm by the milling of $Ba(OH)_2$•$8H_2O$, $Sr(OH)_2$•$8H_2O$ and $Ti(BuO)_4$ in ethanol solution at room temperature. They have homogenous particle grains and high sintering activity. The BST nanoparticles can be sintered as dense ceramics with the density > 90% at a temperature as low ~ 900 $^oC$ with the sintering aids of $Bi_2O_3$ and $Li_2CO_3$ < 5 wt%.

Several Bi-related secondary phases in the ceramics were involved during sintering. Sintering at 800 $^{o}$C, two Bi-related perovskite phases, $SrBiO_3$ and $Ba_2BiO_4$ can be observed. It is realized that $Ba_2BiO_4$ is more difficult to form than $SrBiO_3$, although Ba content is much higher than Sr in BST nanoparticles. The relative content of $Ba_2BiO_4$ vs $SrBiO_3$ increases with the content of the sintering aids. They are both beneficial to the sintering densification. Sintering above 800 $^{o}$C, $SrBiO_3$ disappears. $LiBa_4Bi_3O_{11}$ appears from 830 $^{o}$C, $Sr_{1.2}Bi_{0.8}O_3$ appears from 830 $^{o}$C and disappears above 850 $^{o}$C, and $Bi_{8.11}Ba_{0.89}O_{13.05}$ only appears at 950 $^{o}$C. $LiBa_4Bi_3O_{11}$ and $Sr_{1.2}Bi_{0.8}O_3$ can be regarded as perovskite phases as that of $Ba_2BiO_4$. Sintered at 950 $^{o}$C, the most of alkaline earth cations in Bi-related perovskite impurity phases which driven the sintering densification of the ceramics were resorbed by the main lattice of BST, at the same time $Bi_2O_3$ phase was released again in the end. $SrBiO_3$, $Ba_2BiO_4$, and $LiBa_4Bi_3O_{11}$ might be taken effect on the sintering densification of the ceramics, in which Bi has complex valences. On the other hand, $Sr_{1.262}Bi_{0.737}O_3$ and $Bi_{8.11}Ba_{0.89}O_{13.05}$ might be taken little effect on the sintering densification of the ceramics, in which Bi has a single valence. Sintering at low temperature, the samples have low resistivities due to semiconducting secondary phases, pores, and their distribution on the grain boundary. Sintering at a temperature of $\geq$ 900 $^{o}$C, the ceramics were fabricated with the density > 90%, resistivity > $10^{12}$ Ω·cm, dielectric constant > 6500 at 53 $^{o}$C, and loss < 0.025. The sintering temperature lower to $\leq$ 950 $^{o}$C, the performance of the ceramics will be increased, the energy consumption during ceramic sintering can be decreased and the cost of the devices also will be lowered. The ceramics have a potential for MLCC with silver inner-electrodes.

# References


1. Ezhilvalavan S, Tseng TY, Progress in the developments of (Ba,Sr)$TiO_3$ (BST) thin films for Gigabit era DRAMs, *Mater Chem & Phys* 2000, **65**:227–248
2. Su B, Holmes JE, Cheng BL, *et al.* Processing effects on the microstructure and dielectric properties of barium strontium titanate (BST) ceramics, *J electroceram* 2002, **9[2]** :111-116.
3. Padmini P, Taylor TR, Lefevre MJ, *et al.* Realization of high tunability barium strontium titanate thin films by rf magnetron sputtering, *App Phys L* 1999, **75[20]** : 3186-3188.
4. Tombak A, Maria JP, Ayguavives F, *et al.* Tunable barium strontium titanate thin film capacitors for RF and microwave applications, *IEEE Microwave and wireless components letters*, 2002, **12[1]**:3-5.
5. Nath R, Zhong S, Alpay SP, *et al.* Enhanced piezoelectric response from barium strontium titanate multilayer films, *App Phys L* 2008, **92[1]**:012916.
6. Huck C, Poghossian A, Bäcker M, *et al.* Capacitively coupled electrolyte-conductivity sensor based on high-k material of barium strontium titanate, *Sens & Act B: Chem* 2014, **198** :102-109.
7. Sauer HA, Flaschen SS, Hoesterey DC. Piezoresistance and piezocapacitance effects in barium strontium titanate ceramics, *J Am Ceram Soc* 1959, **42[8]** :363-366.

8. Wei X, Vasiliev AL, Padture NP, Nanotubes patterned thin films of barium-strontium titanate, *J Mater Res* 2005, **20[8]**:2140-2147.
9. Gorzkowski EP, Pan MJ, Bender B, *et al.* Glass-ceramics of barium strontium titanate for high energy density capacitors, *J electroceram* 2007, **18[3-4]**:269-276.
10. Qi JQ, Chen WP, Wu YJ, *et al.* Improvement of the PTCR Effect in $Ba_{1-x}Sr_xTiO_3$ Semiconducting Ceramics by Doping of $Bi_2O_3$ Vapor during Sintering, *J Am Ceram Soc* 1998, **81**:437-438.
11. Li J, Jin D, Zhou L, *et al.* Dielectric properties of Barium Strontium Titanate (BST) ceramics synthesized by using mixed-phase powders calcined at varied temperatures, *Mater L* 2012, **76** :100-102.
12. Yu Z, Sergeant NP, Skauli T, *et al.* Enhancing far-field thermal emission with thermal extraction, *Nature comm* 2013, **4[1]**:1-7.
13. Jiang TH, Zhai WJ, Chou JX, *et al.* Influence of $Bi_2O_3$ and CuO addition on low-temperature sintering and dielectric properties of $Ba_{0.6}Sr_{0.4}TiO_3$ ceramics, *Mater Res Bul* 2009, **44[3]**:566-570.
14. Tick T, Peräntie J, Jantunen H, *et al.* Screen printed low-sintering-temperature barium strontium titanate (BST) thick films, *J Eu Ceram Soc* 2008, **28[4]** :837-842.
15. Qi JQ, Wang Y, Chen WP, Li LT, *et al.* Direct synthesis of ultrafine tetragonal $BaTiO_3$ nanoparticles at room temperature, *Nanoscale Res L* 2011, **6[1]** :466.
16. Khazraie A, Foyevtsova K, Elfimov I, Oxygen holes and hybridization in the bismuthates, *Phys Rev B* 2018, **97[7]** :075103.
17. Foyevtsova K, Khazraie A, Elfimov I, *et al.* Hybridization effects and bond disproportionation in the bismuth perovskites. *Phys Rev B* 2015, **91[12]**: 121114.
18. Licheron M, Gervais F, Coutures J, *et al.* "$Ba_2BiO_4$" surprisingly found as a cubic double perovskite $Ba_2$ ($Ba_{23}Bi_{13}$) $BiO_{6-\delta}$. *Sol State comm* 1990, **75[9]** :759-763.
19. Fang L, Hu CZ, Guo RL, *et al.* Low temperature sinterable microwave ceramics of $LiBa_4Bi_3O_{11}$ and their fabrication, *Chinese Patent* 2012, CN102531568A
20. Yu D, Zhao M, Wang C, *et al.* Amorphous phases and composition dependence of piezoelectricity in $BaTiO_3$-$Bi_2O_3$ polar amorphous ceramics, *Ceram Inter* 2016, **42[1]**:1777-1781

# Figures

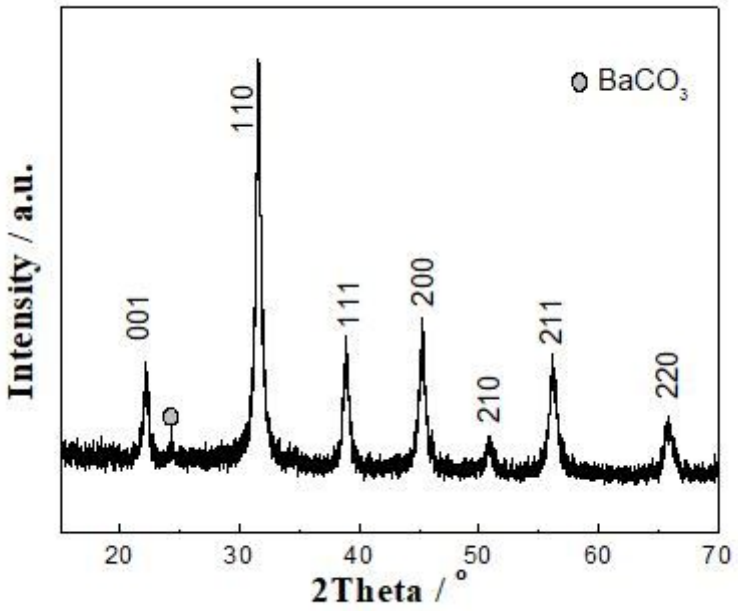


## Figure 1

XRD pattern of BST powders synthesized at room temperature

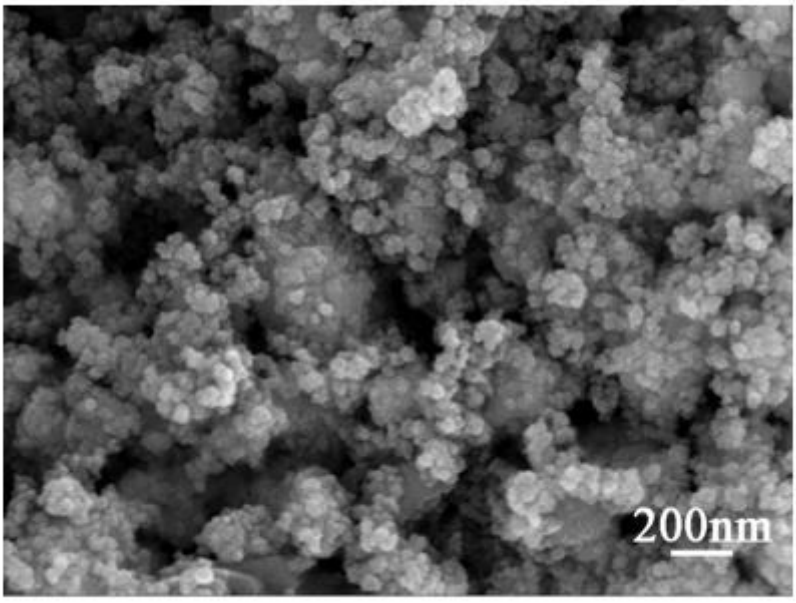


## Figure 2

SEM of BST nanoparticles directly synthesized at room temperature


**Figure 3**

samples sintered at 800 oC for 8 h with different contents of sintering aids

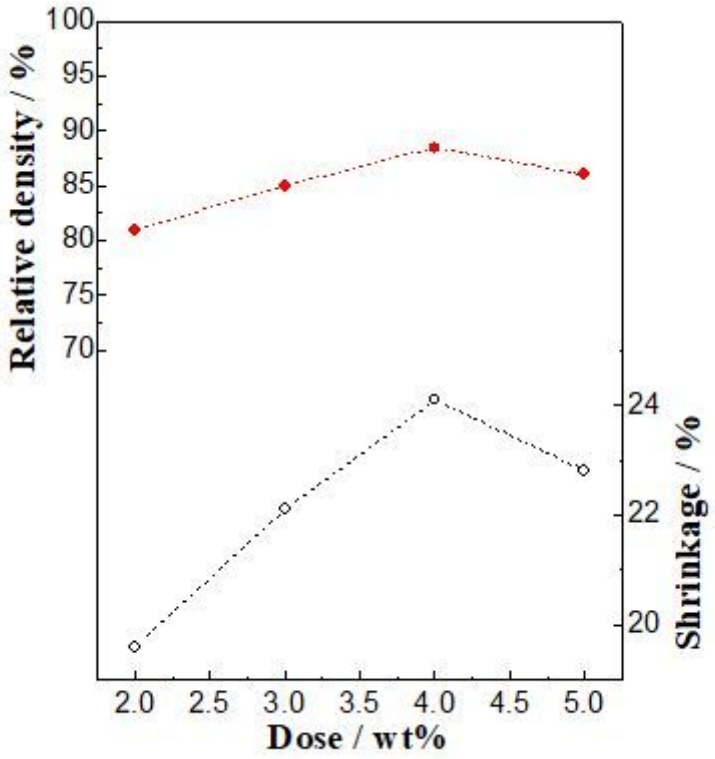


**Figure 4**

Relative density and sintering shrinkages of the samples sintered at 800 oC for 8 h with different contents of sintering aids

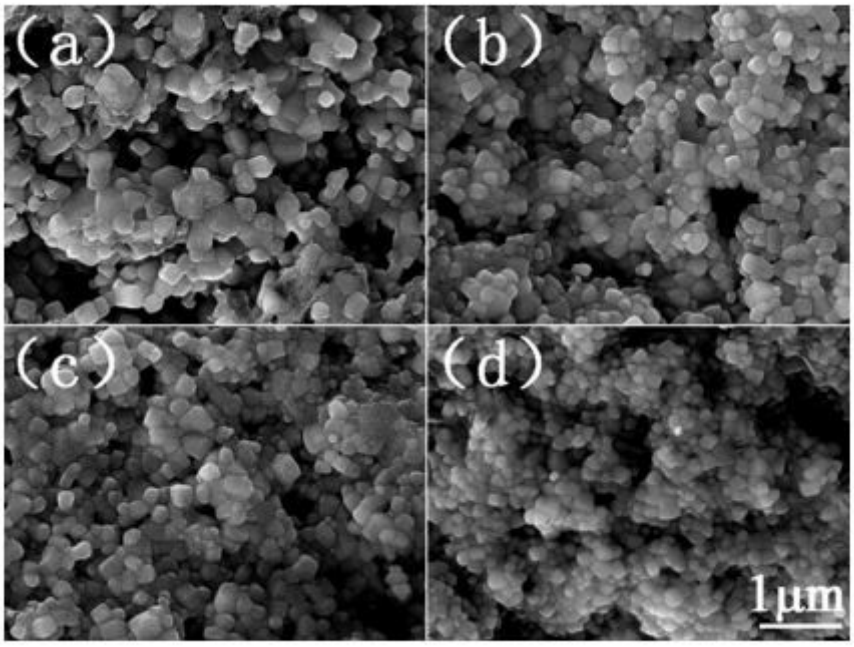


**Figure 5**

SEM of the samples sintered at 800 oC for 8 h with different contents of sintering aids (all images have the same scale bar), (a) 2 wt% (b) 3 wt%, (c) 4 wt%, (d) 5 wt%

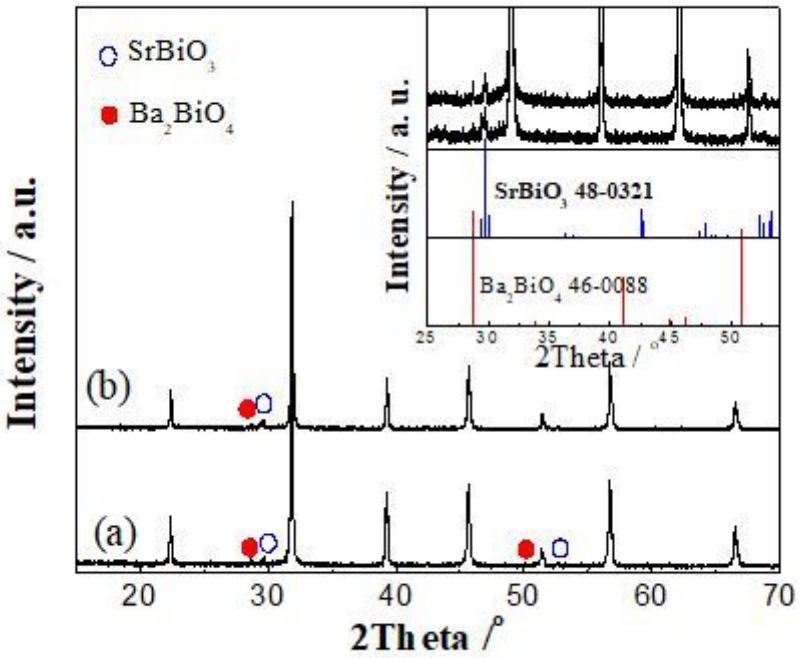


**Figure 6**

XRD patterns of the samples sintered at 800 oC for 8 h with the sintering aids of (a) 3 wt%, (b) 5 wt%


Figure 7

samples sintered at a different temperature with 3 wt% sintering aids

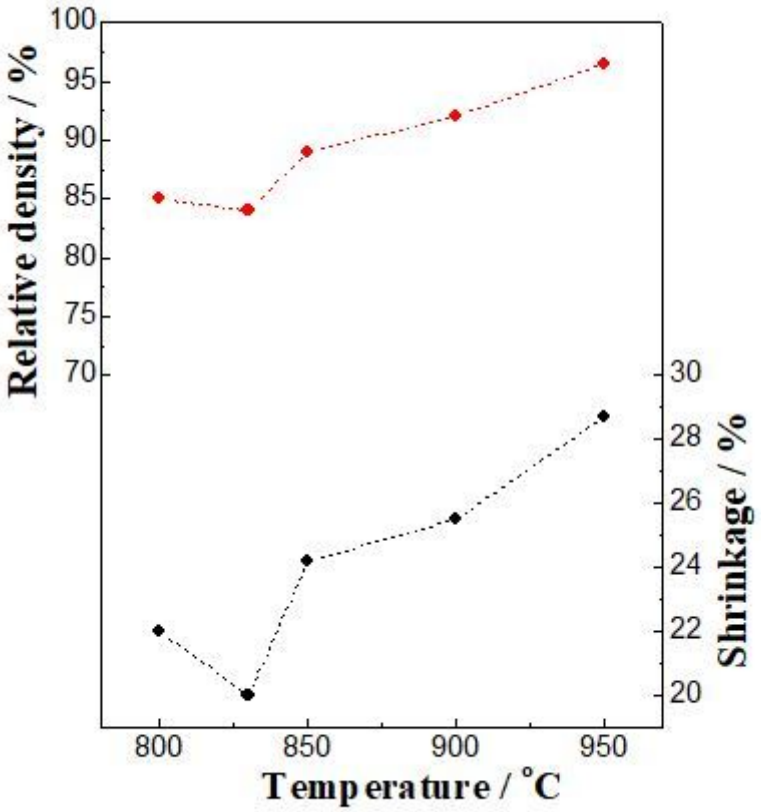


Figure 8

Relative density and sintering shrinkages of the samples sintered at different temperatures for 8 h with 3 wt% sintering aids

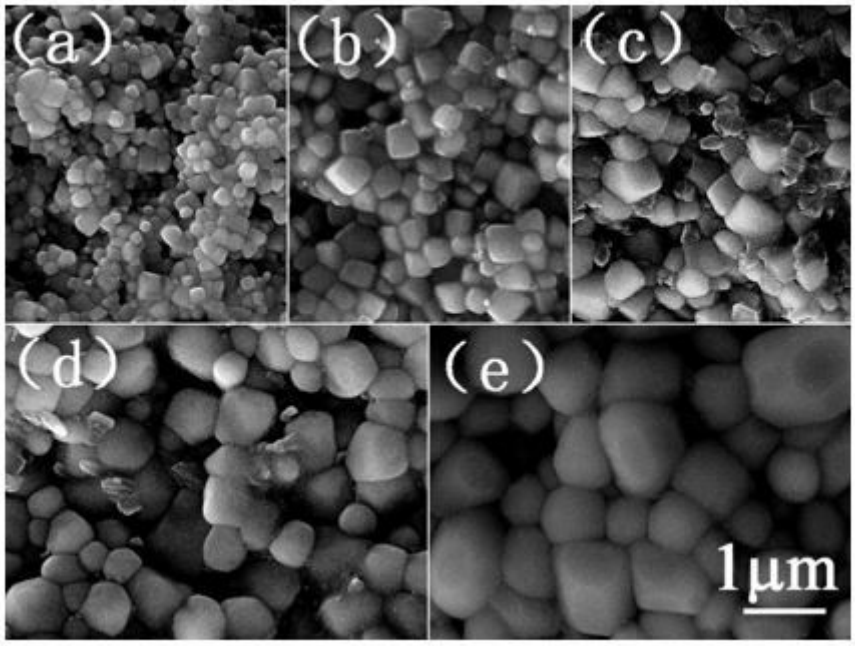


**Figure 9**

SEM of the samples sintered at different temperatures for 8 h with 3 wt% sintering aids (all images have a same scale bar), (a) 800 oC, (b) 830 oC, (c) 850 oC, (d) 900 oC, (e) 950 oC

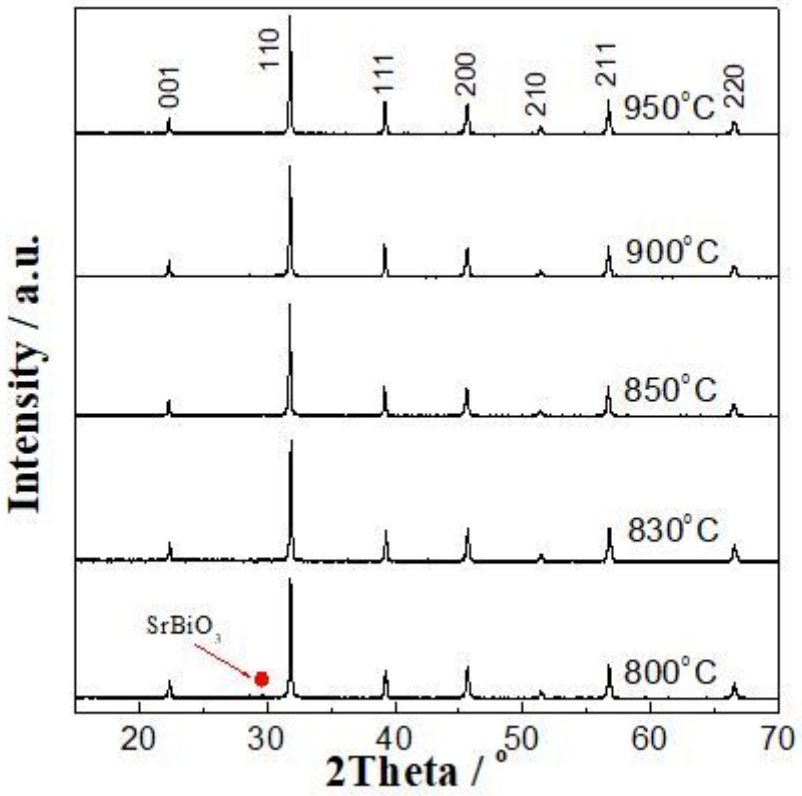


**Figure 10**

XRD patterns of the samples sintered at different temperatures for 8 h with 3 wt% sintering aids

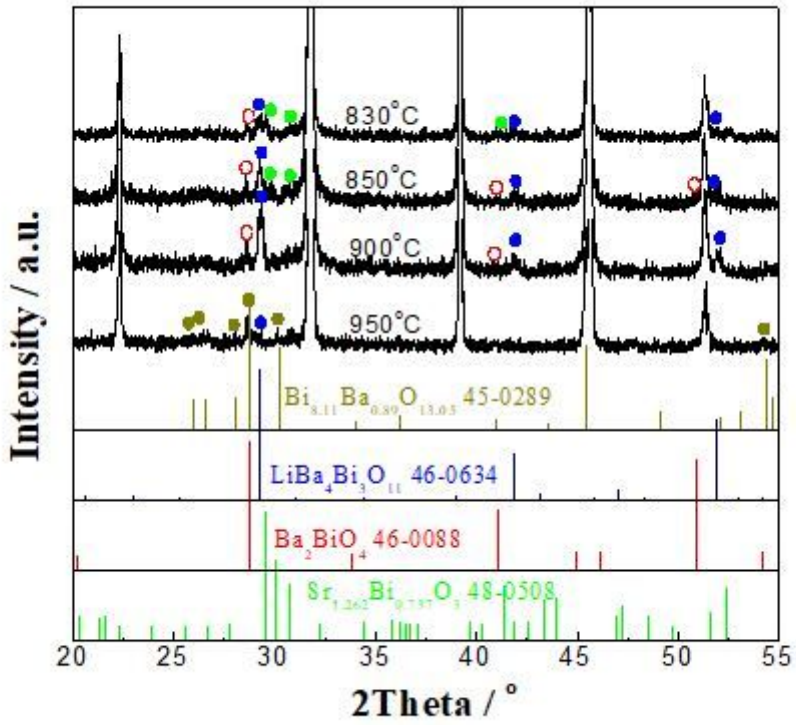

## Figure 11

XRD patterns of the samples sintered at different temperatures for 8 h with 5 wt% sintering aids

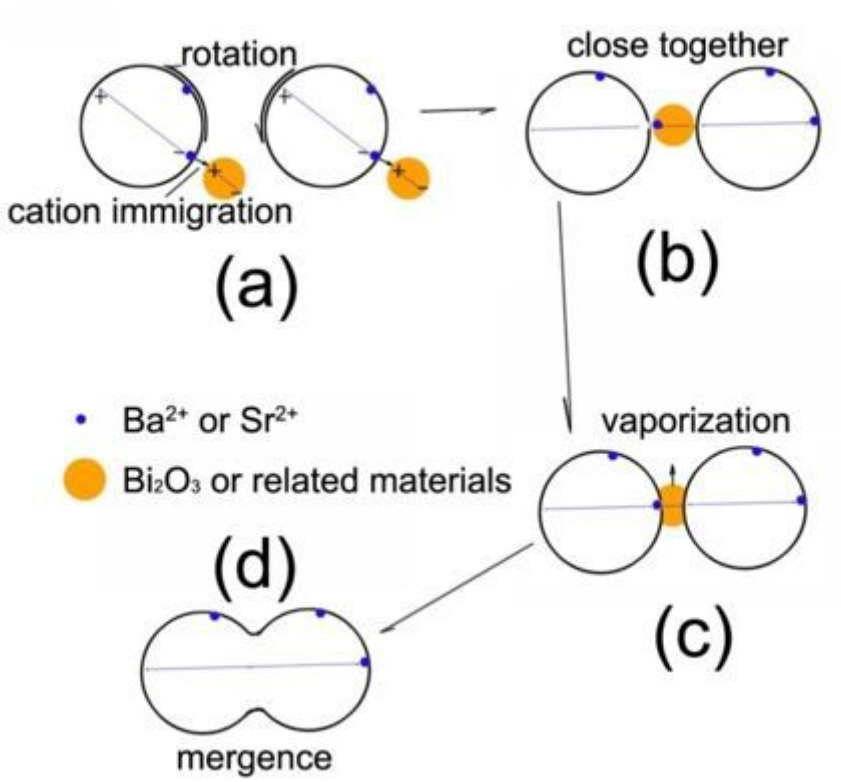


## Figure 12

Illustration of the sintering mechanism

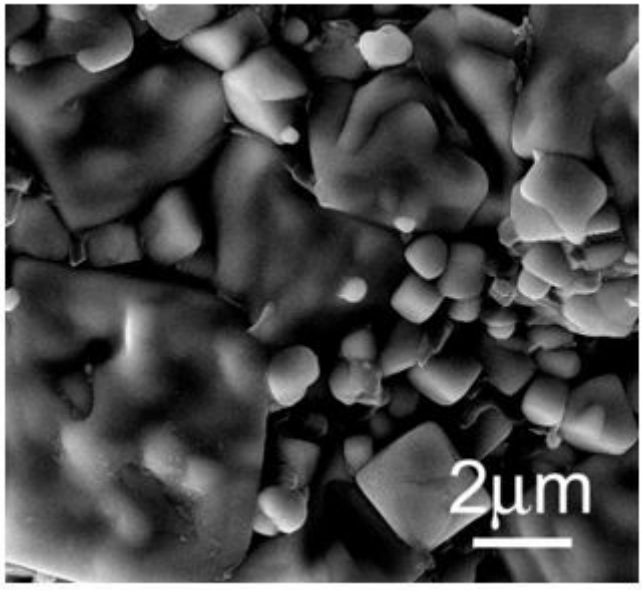

## Figure 13

Small particles merged into large grain during sintering, SEM of the samples sintered at 950 oC for 2 h with 5 wt% sintering aids

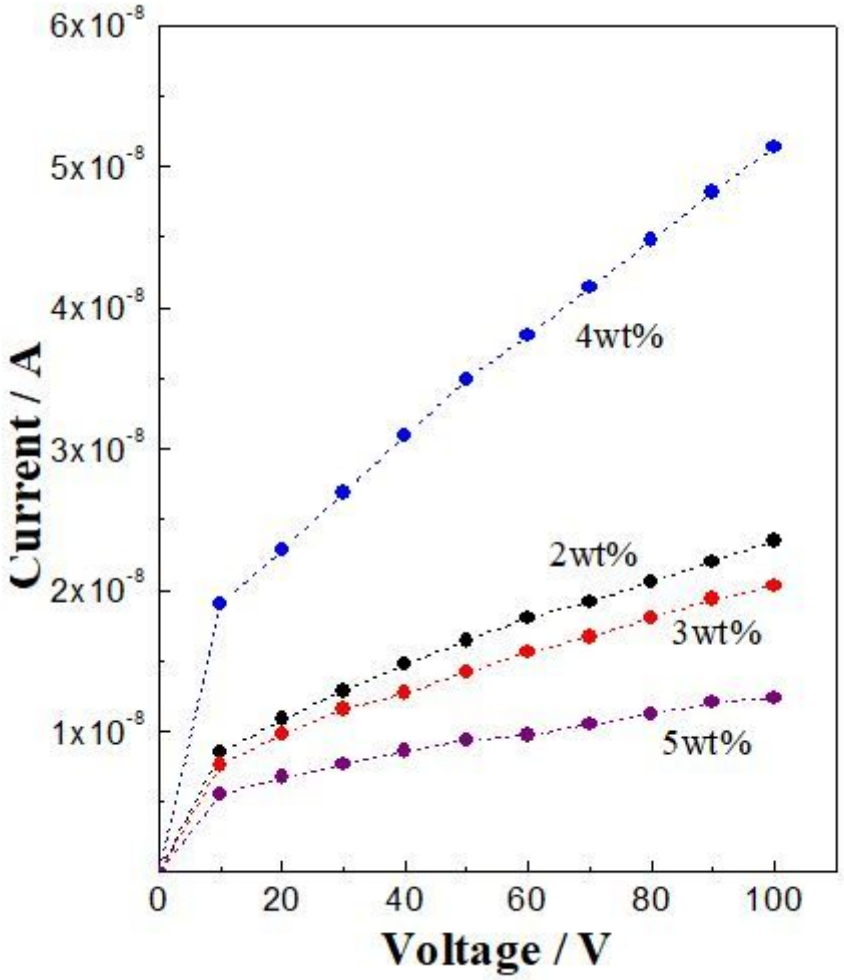


## Figure 14

I-V curves of the samples sintered at 800 oC for 8h with the different sintering aids

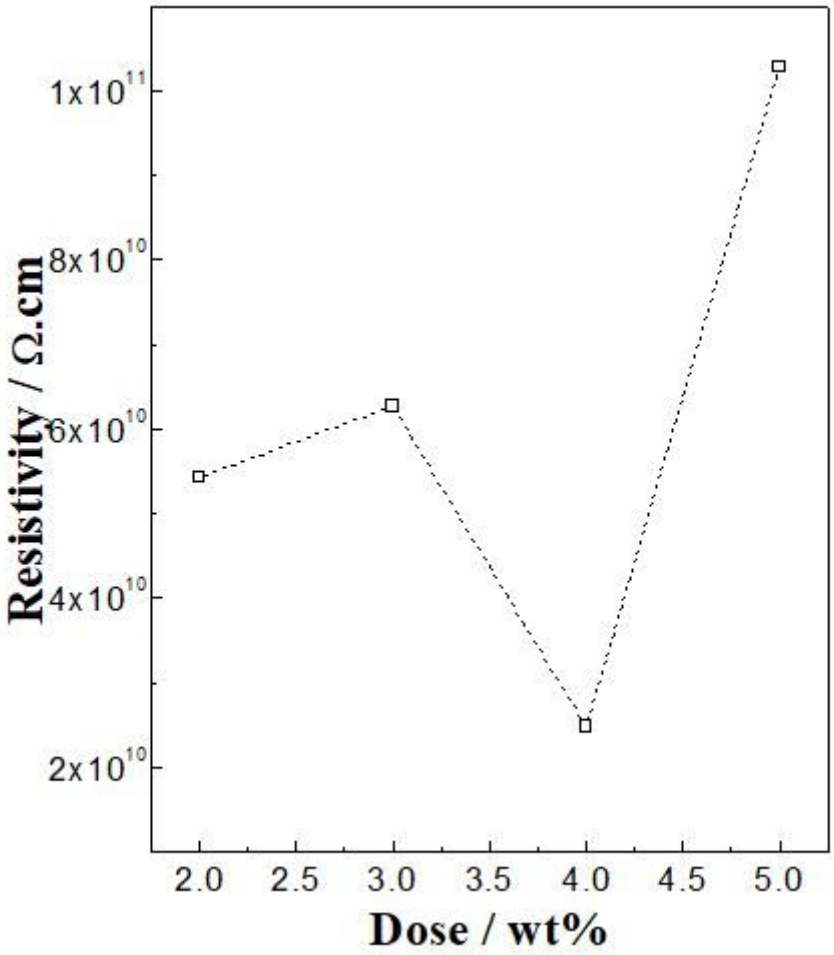


## Figure 15

I-V Resistance of the samples sintered at 800 oC for 8 h with different content of sintering aids

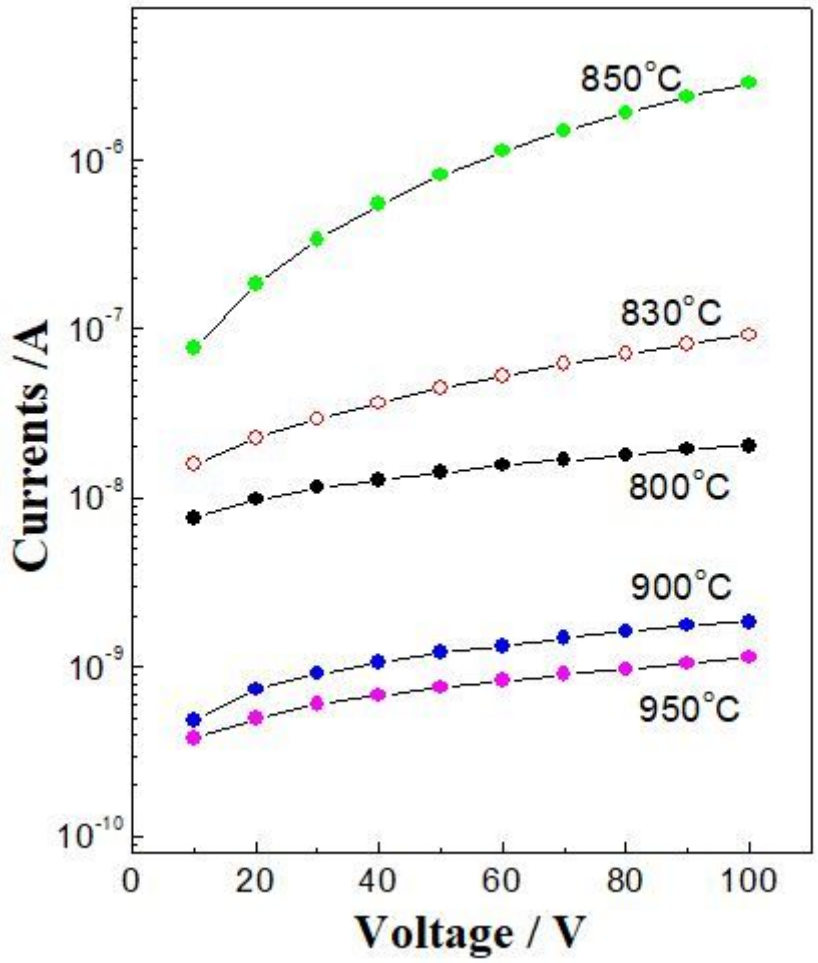


## Figure 16

I-V curves of the samples sintered at a different temperature with 3 wt% sintering aids

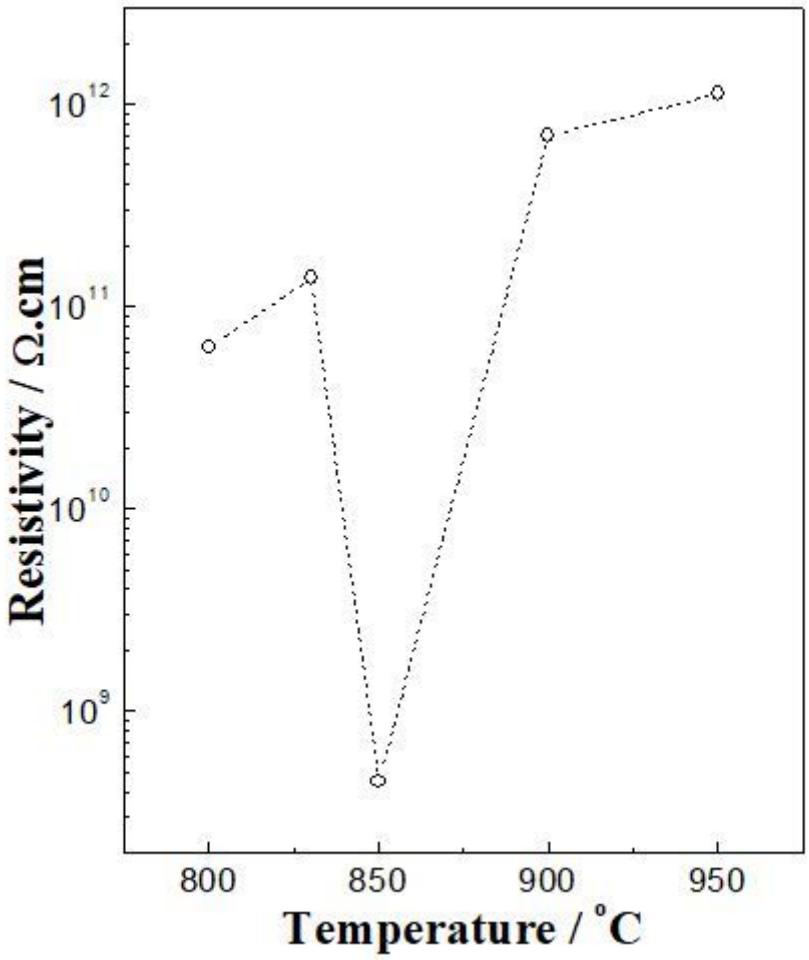


**Figure 17**

Resistance of the samples sintered at a different temperature with 3 wt% sintering aids

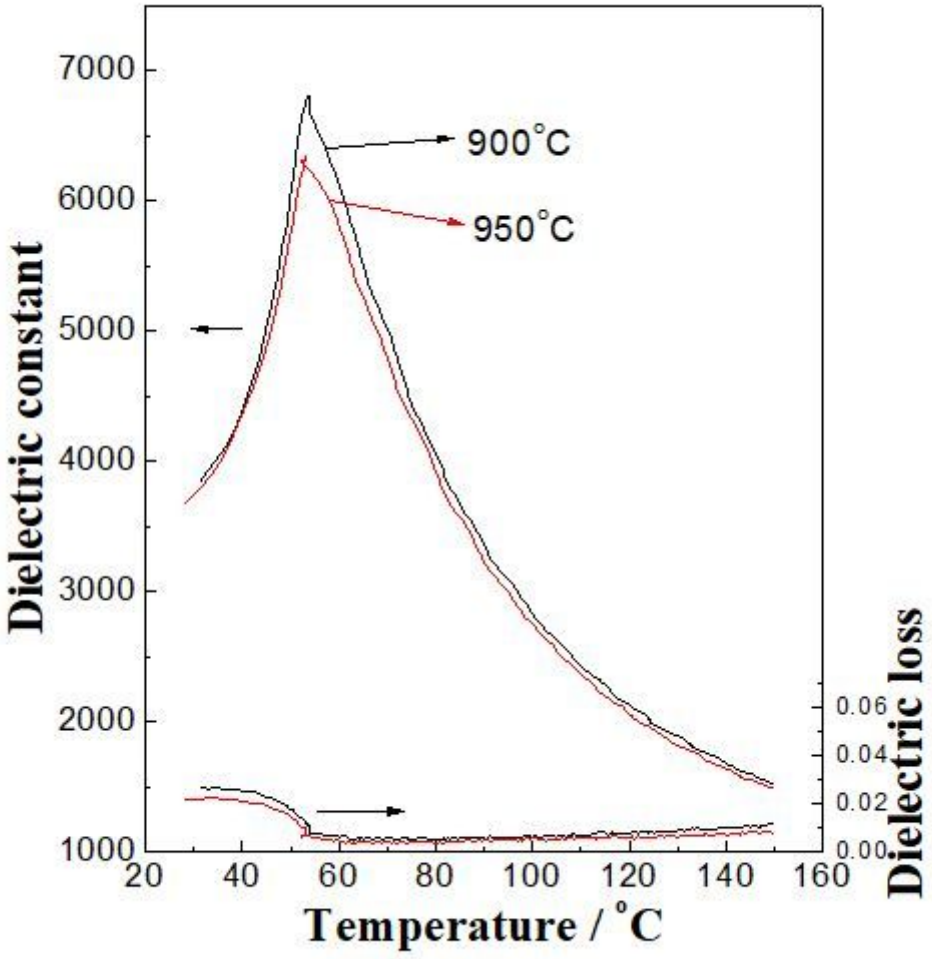


## Figure 18

Temperature dependence of dielectricity of the samples sintered at 900 oC and 950 oC